Letter

Broad photoluminescence from large Frank-Condon relaxation dynamics of hole polarons in LiGaO$_2$

Manoj Dey and Abhishek Kumar Singh[*]

Materials Research Centre, Indian Institute of Science, Bangalore 560012, India

The broad and Stokes-shifted photoluminescence line in ultra-wide-band gap semiconductors has numerous potential applications starting from white light generation, nanoscale optical thermometers to quantum information readout. Here, using density functional theory with an effective U approach and hybrid functional study, we establish the correlation between self-trapped hole polaron relaxation dynamics and broadness in photoluminescence spectra of ultra-wide-band gap oxide LiGaO$_2$. After electron capture, self-trapped hole undergoes large lattice relaxation and gives rise to a broad and strongly Stokes-shifted emission band peaking at 4.17 eV. The donated holes from single acceptor defects form tightly bound states and serve as deep defects. These defects also provide additional stability to bound hole polarons and produce broader luminescence bands, with peaks in the infrared to the visible range of 2.4–4.1 eV. Our findings shed light on the fundamental properties of ultra-wide-band gap semiconductor oxides and provide insights into strategies for tuning luminescence bands for future optoelectronic applications.

Ultra-wide-band gap semiconductors have emerged as front-runners for various applications, including high-power electronics, deep ultraviolet optoelectronics, and solid-state lighting [1–3]. Free exciton recombination results in narrow emission, which is beneficial for pure-color production in light-emitting diodes [4,5]. Broad and highly Stokes-shifted emission, on the other hand, has the potential to produce white light [6,7]. The temperature dependence of linewidth and peak shift in wide luminescence spectra could be utilized to create nanoscale optical thermometers [8]. Furthermore, optically active defect centers at ultra-wide-band gap semiconductors serve as the foundation for quantum information technology [9]. The ultra-wide-band gap accommodates deep center defects while ensuring that the optical transition does not interfere with host electronic states. The interaction of quasiparticle and vibronic modes near deep center defects often leads to phonon-assisted broadening, which is useful for read-out quantum information [10]. Therefore, precisely recognizing the optical signature of deep center defects could assist in employing ultra-wide-band gap semiconductors in potential applications.

Gr-I-III-IV$_2$ oxide lithium gallate (LiGaO$_2$) has ultra-wide-band gap (5.1–5.3 eV), even larger than β-Ga$_2$O$_3$. LiGaO$_2$ exhibits ultralong near-infrared persistent photoluminescence (PL) that lasts much longer than 26 hours [11]. The best value of external quantum efficiency can be achieved up to 50.8 % when LiGaO$_2$ is used as the substrate [12]. Despite having the potential for future optoelectronic applications, the origin of optical signature in LiGaO$_2$ is poorly understood. LiGaO$_2$ exhibits several broad luminescence lines attributed to deep center defects, with the emission band ranging from 1.77 to 4.43 eV [13–15]. Notably, Hsiao *et al.* [16] reported strong

and broad emission peaks at 3.24 eV (383 nm) from LiGaO$_2$ nanoflakes, while Yanagida *et al.* [17] observed a broad photoluminescence band center at 3.65 eV (340 nm). Other studies have reported green luminescence in Cu-doped LiGaO$_2$ at 3.81 eV [18], broad ultraviolet emission peaks at 4.39 and 3.64 eV, along with green-yellow peaks at 1.92–2.29 eV [19]. Despite numerous reports, critical questions still remain about the atomistic origins and underlying mechanisms of the observed luminescence lines, along with why they are all broad in nature.

In order to address these, we perform first-principles calculations and explicitly correlate the hole polaron relaxation dynamics with the origin and broadness of photoluminescence spectra. The excess hole gets localized as the hole polaron in the O-p orbital owing to the polarization potential created by lattice distortion around O site. The electron captured by self-trapped hole polaron during photoexcitation results in significant vibrational broadening and high reorganization energy. This, in turn, leads to a broad and strongly Stokes shifted photoluminescence in the ultraviolet region (4.17 eV). Interestingly, all the acceptor impurities constitute a tightly bound hole polaron and act as deep center defects. Electron capture by the bound hole polarons with the defects also shows broader photoluminescence spectra peaking from infrared to visible region of the spectrum. The acceptor dopants provide additional stability to bound holes by increasing the lattice distortion and further broadens the photoluminescence spectra.

A self-trapped polaron forms when an excess electron or hole deforms the crystal lattice, thereby creating a potential well that traps it. Single acceptor defects provide holes, which typically prefer to form small polarons, rather than existing as delocalized holes in ionic or polar semiconductor. Oxides frequently exhibit asymmetric localization of acceptor-bound holes at multiple comparable oxygen sites [20]. Moreover,

*abhishek@iisc.ac.in

density functional theory (DFT) with conventional (semi)local approximations often cannot tackle wide band gap oxides owing to well-known self-interaction errors [21]. In order to properly account for self-interaction corrections, we first satisfy the generalized Koopmans condition using the cancellation of nonlinearity approach as suggested by Lany *et al.* [20]. All the DFT calculations are performed with Vienna *Ab initio* Simulation Package (VASP [22]). The linearity of total energy with fractional occupation number is reached using Heyd, Scuseria, and Ernzerhof (HSE) hybrid functional with 0.1 Å^{-1} screening and 25% mixing, and DFT + U with U = 8 eV (see Supplemental Material (SM) [23] for details, see also Refs. [24–34] therein). To reduce the computational cost, we first employed the DFT + U formalism for establishing the hole polaron model, as identifying acceptable lattice distortion for polarons requires a random search. We adopted the HSE hybrid functional for the rest of the work after confirming the hole polaron stabilization. The extended computational details about the first-principles calculations and information about atomic and electronic structures are provided in the SM [23].

Pure LiGaO$_2$ shows insulating behavior because of the pinning of Fermi level deep in the gap [35]. Though *n*-type doping is possible with Si and Ge dopants, achieving *p*-type dopability is hard in LiGaO$_2$ owing to heavy hole masses [36]. Like several transition metal oxides, LiGaO$_2$ also has a tendency to trap holes in self-polarizing field to form small polarons. Electron paramagnetic resonance (EPR) study suggests that singly ionized lithium vacancies (V$_{Li}^0$) and doubly ionized gallium vacancies (V$_{Ga}^{-2}$) show bound small polarons [37]. The recent study also demonstrates the localized polarons at nearest oxygen site of Li and Ga vacancy using *g* tensors and superhyperfine interaction calculations [38]. In order to investigate the hole polaron formation, we first remove one electron from LiGaO$_2$ 2 × 2 × 2 supercell and relax the system in the presence of charge neutralizing background. The extra hole gets delocalized and forms Bloch-like extended state [isosurface of hole density is shown in Fig. 1(a)]. In contrast, the localized polaronic state forms when starting with a small initial perturbation (stretching O-Li and O-Ga bonds by ≈ 8%) around a selected O atom. The hole gets localized in O-2*p* orbital with spin S = 1/2 configuration. The oxidation state also changes from O^{-2} to O^{-1}. This O^{-1} species is usually found by EPR experiments in Ga-based oxides, including LiGaO$_2$ [37,39]. The localized hole polaron is more stable than the Bloch-like extended state by 0.40 eV (using DFT + U with U = 8 eV). After the confirmation of the stabilization of the hole polaron, we determine the formation energy of hole polaron using HSE (0.10, 0.25) functional. The hole polaron formation energy in grand-canonical formulation for defects [40], can be calculated as

$$\Delta E_{hole}^{free} = E_{hole}^{+1} - E_{pris}^0 + \epsilon_{VBM} + \Delta E_{corr}(+1), \quad (1)$$

where, E$_{hole}^{+1}$ and E$_{pris}^0$ are the total energy of the supercell containing a small hole polaron and pristine neutral supercell, respectively. The ϵ_{VBM} is the reference bulk valance band maxima (VBM). The finite-size electrostatic charge correction is included by using extended anisotropic Freysoldt-Neugebauer-Van de Walle (FNV) scheme [41,42]
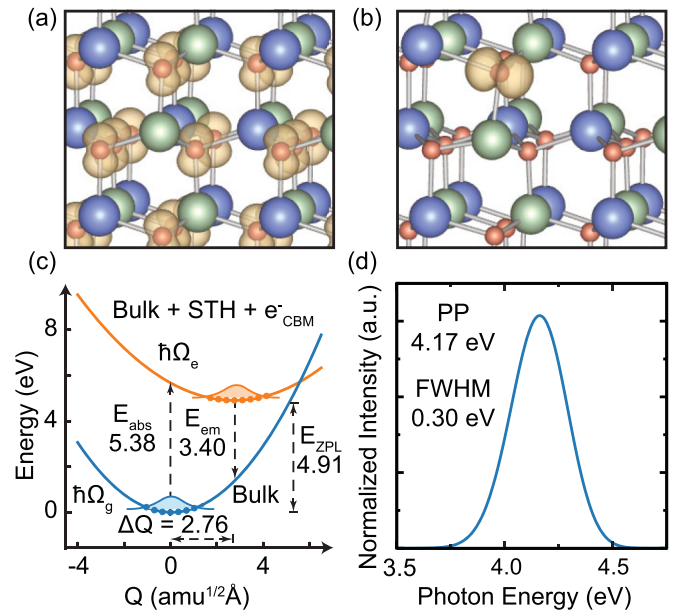
FIG. 1. (a) Isosurface plot of hole density of completely delocalized Bloch-like extended state in the undistorted structure. In the ball and stick model, Li, Ga, and O atoms of LiGaO$_2$ are shown in blue, green, and red, respectively. (b) The localized hole polaron is confined in an O atom. The isosurface plot of localized hole density is shown in yellow and has O-2*p* orbital nature. Isosurface value set to 10% of maximum for both delocalized and localized hole state. (c) 1D configuration coordinate diagram for describing the electron capture process by the self-trapped hole (STH). The dots are computed potential energies from first principles, and the solid lines represent their corresponding quadratic spline interpolation or extrapolation. The absorption (E$_{abs}$), emission (E$_{em}$), and zero-phonon line (E$_{ZPL}$) have units of eV. ΔQ is the change in generalized coordinate during the relaxation process, and Ω$_{g/e}$ is the effective phonon frequency in the ground and excited states. (d) Simulated broad luminescence line of corresponding optical transition of electron capture from conduction band minima. The peak position (PP) and full width at half maximum (FWHM) are mentioned.

with the static dielectric constant (ϵ_0, see SM [23]). The corresponding free hole polaron formation energy is −0.19 eV.

The self-trapped hole polaron formation can be represented as O$_O^+$ in defect notations, as the local structural environment of the localized site is nonequivalent to the other O sites. The hole polaron formation energy then corresponds to E$_f$[O$_O^+$] at the Fermi level located at the VBM as shown in Fig. 2(b). Therefore, the hole polaron is stable when the Fermi level is lower than 0.19 eV with respect to VBM. In other words, the photoexcitation of electron to conduction band leaves a hole in the VBM. The extra hole gets localized, accompanied by local lattice distortion, and forms a stable small hole polaron. The capture of an electron from the conduction band minima (CBM) to the localized hole level will give a luminescence line. The self-trapping potential is considered fixed during the photoexcitation process since the movement of the atoms surrounding the polarons that produce the potential well is slower than photoexcitation. As a result, the Frank-Condon principle can be applied. The zero phonon line energy (E$_{ZPL}$) corresponding to polaron formation energy is 4.91 eV. Optical
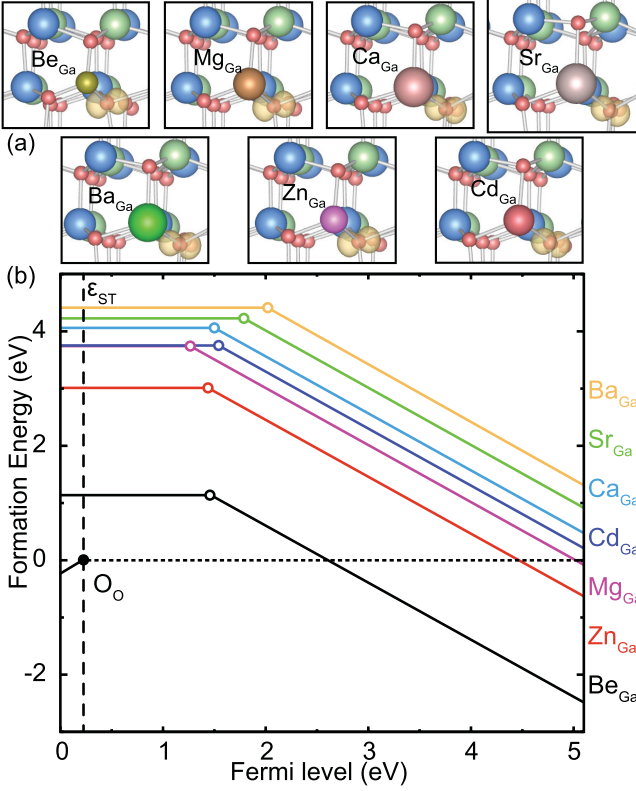
FIG. 2. (a) Relaxed structures of Gr. II (Be, Mg, Ca, Sr, and Ba) and Gr. XII (Zn and Cd) substitution at Ga site acceptor bound hole polaron in ball-stick model. The isosurface value of hole density is set to 10% of maximum. (b) Formation energy as a function of Fermi level for all acceptor impurities. The Fermi level ranges from the VBM to the CBM. Slopes indicate the charge state of defect, and kinks in the curves correspond to charge-state transition levels. The hole polaron formation is denoted as O_O. ϵ_{ST} is the self-trapping energy up to which the hole polaron is stable above VBM.

transitions are vertical in the Franck-Condon approximation, which implies the emission and absorption energies can be described as $E_{em} = E_{ZPL} - \Delta E_g^{FC}$; $E_{abs} = E_{ZPL} + \Delta E_e^{FC}$; where, ΔE^{FC} is Frank-Condon relaxation energy. To investigate the optical transition involving the self-trapped hole, we adopt the one-dimensional configuration coordinate diagram (1D CCD) approach, as implemented in Nonrad [43]. The 1D CCD model in Fig. 1(c) describes the electronic and vibronic properties of polaron corresponding to optical excitation. We calculated normalized luminescence line shape from spectral function of this transition [Fig. 1(d)], using the following equation [44]:

$$G(\hbar\omega) = C\omega^3 \sum_{m,n} w_m(T)|\langle \chi_{fm}|\chi_{in}\rangle|^2$$
$$\times \delta(E_{ZPL} + \hbar\omega_{fm} - \hbar\omega_{in} + \hbar\omega), \quad (2)$$

where C is the normalization factor and $w_m(T)$ is the thermal occupation of the final phonon state. $\langle \chi_{fm}|\chi_{in}\rangle$ is the overlap integral of initial and final ionic wave functions. Complete details can be found in Ref. [44]. This approach is successfully implemented to study the luminescence property of deep defects with strong electron-phonon interaction [45–50]. The

TABLE I. Binding energy (E_{bind}) of hole polarons with acceptor impurities, ionic radius difference of dopants (r_x) with Ga (r_{Ga}), and mass-weighted lattice distortion (ΔQ) for hole polarons formation.

	Be_{Ga}	Mg_{Ga}	Ca_{Ga}	Sr_{Ga}	Ba_{Ga}	Zn_{Ga}	Cd_{Ga}
E_{bind} (eV)	1.30	1.07	1.30	1.59	1.83	1.26	1.35
$|r_x - r_{Ga}|$ (pm)	17	10	38	56	73	12	33
ΔQ (amu$^{1/2}$Å)	2.42	2.70	2.91	4.07	3.31	1.84	2.38

peak position of the corresponding transition from CBM to localized hole is at 4.17 eV. A similar luminescence line due to carrier recombination is also observed at 3.77 eV and 4.43 eV in LiGaO$_2$ in pump-probe experiments [13]. The observed 3.76 eV (330 nm) band has been attributed to the presence of hole in the oxygen site [14]. The calculated parameters (discusssed in the SM [23]) from the configuration coordinate diagram are tabulated in Table S3 in the SM [23]. A lattice distortion created by the self-trapped hole polaron results in vibrational broadening, which corresponds to large Franck-condon shifts. The high reorganization energy during photoexcitation also explains the Stokes' shift and emission line width. The corresponding Franck-Condon relaxation energies in the ground and excited states are 1.51 and 0.47 eV, respectively. As a result, the luminescence band becomes broad with a full width at half maximum (FWHM) of 0.30 eV.

Having established the hole polaron model and origin of the broad photoluminescence band, we further investigate the effect of bound hole polarons on luminescence spectra in the presence of acceptor defects. We consider Gr. II (Be, Mg, Ca, Sr, and Ba) and Gr. XII (Zn and Cd) acceptor impurities. The donated hole from all the acceptor impurities forms a bound hole polaron at the nearest O-sites [see Fig. 2(a)]. The binding energy of the hole polaron with the acceptor can be calculated from the energy difference between localized and free hole polaron as (tabulated in Table I),

$$E_{bind} = \Delta E_{hole}^{free} - \Delta E_{hole}^{bound}. \quad (3)$$

Among all, Ba has the highest hole polaron binding energy of 1.83 eV and Mg has low binding energy followed by Zn. We note that the contribution of ionic size difference at Ga site has a large impact on binding hole polarons. Mg has a smaller ionic radius difference of 10 pm with Ga, followed by Zn, whereas, the difference is large for Ba. Therefore, the large ionic size difference of acceptor impurities at the incorporation site increases lattice distortion and assists in forming a bound polaron. In other words, acceptor impurities provide additional stability in terms of lattice distortion to form hole polarons. To quantify the lattice distortion during hole polaron formation, we determined the change in the generalized coordinate as $\Delta Q = \sqrt{\sum_\alpha m_\alpha (\Delta R_\alpha)^2}$; where ΔR_α is the displacement from equilibrium of all the atoms α with mass m_α. The displacement of heavy dopants along with ionic size differences, contribute largely to lattice distortion. The high value of ΔQ also demonstrates the significant coupling between the hole and lattice distortion during localization.

We now calculate the defect formation energies (see SM [23] for definition) of all the acceptor defects to determine the thermodynamic stability. We consider the Ga-poor, O-rich

condition ($\Delta\mu_{Ga} = -5.74$ eV, $\Delta\mu_O = 0$ eV) in the phase diagram (shown in Fig. S3 in SM [23]) for calculating formation energies as it is the most favorable for incorporation of acceptor impurities at Ga site. Figure 2(b) shows the formation energy and charge transition level for all the Gr. II and Gr. XII acceptor impurities. Be_{Ga} has the lowest formation energy, followed by Zn_{Ga}. This can be attributed to the small ionic size of Be. Recently, the dual nature behavior of shallow acceptor state and strong localized small polaron state formation is found with Be doping in GaN [51]. Therefore, further experimental investigation is required to determine the nature of the Be doping as it is the most viable defect in $LiGaO_2$. Zn_{Ga} has 2 eV higher formation energy than Be_{Ga}. Moreover, Ba_{Ga} has the highest formation energy because of the larger ionic size. Figure 2(b) demonstrates that $(0/-1)$ transition levels for all the acceptors are very deep. Among them, Mg_{Ga} has the lowest acceptor level, lying 1.25 eV above VBM. Zn_{Ga} has 0.22 eV deeper acceptor level at 1.47 eV. Therefore, the possibility of achieving p-type dopability is very less because of the bound hole polaron formation. We note that the possibility of impurities incorporation depends on the growth condition, i.e., the chemical potential of constituent. Moreover, the formation energy of each acceptor depends on the electronic chemical potential (i.e., Fermi level). Some acceptor impurities (Be, Zn, and Mg) have a negative while others have lowest formation energy when Fermi level is very close to CBM. Therefore, in a typical n-type condition, all the impurities have a tendency to accept one electron and become stable in its negative charge state. The electrons will also be compensated in the presence of shallow donor defects and pin the Fermi level deep below the CBM, depending upon the formation energy of the donor and acceptor defects. Therefore, if we try to grow n-type $LiGaO_2$ in the presence of acceptor impurities, the n-type conductivity will be compensated, and the material will behave as semi-insulating. $LiGaO_2$ has a similar crystal structure and very little lattice mismatch with GaN [19,52] and ZnO [53] in different cleaved surfaces. Therefore, $LiGaO_2$ can be used as a very good buffer layer in GaN and ZnO-based power electronic devices.

After understanding defect thermodynamics, we study the photoluminescence property of these deep defects. The defect-assisted photoexcitation and luminescence mechanisms are shown in Fig. 3. In a typical n-type grown sample, the $(0/-1)$ level of deep defect is occupied by one electron when the Fermi level is higher than the defect level [Fig. 3(a)]. The electron capture will lead to the formation of X_{Ga} (X = Be, Mg, Ca, Sr, Ba, Zn, and Cd) defect in a -1 charge state, where hole polaron level is compensated by an electron. This electron can be excited to CBM via photoexcitation, and the defect will change its charge state. According to the Frank-Condon principle, the defect will be in the initial configuration during the photoexcitation. The variation of the structural configuration is described by 1D CCD as shown in Fig. 3(b). After the photoexcitation, the defect will undergo a structural change by forming a defect-bound hole polaron. The defect configuration then relaxes to $X_{Ga}^0 + e_{CBM}$ structure with some relaxation energy leaving the electron in the CBM (minima of the orange parabola). Typically, this relaxation energy is very high because of the formation of localized bound hole polaron. The electron comes back to the $(0/-1)$
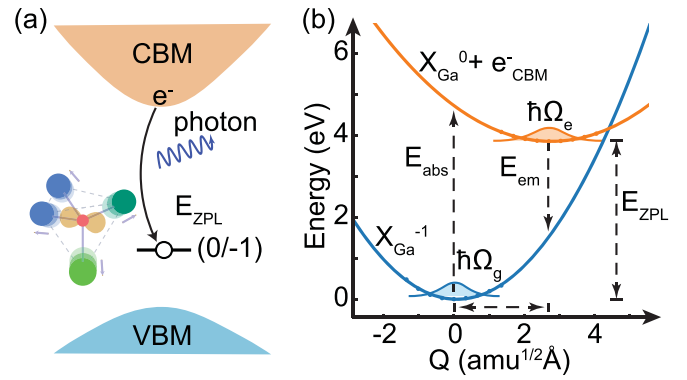
FIG. 3. (a) Defect bound hole polaron assisted optical transition by electron capturing at acceptor level. The inset shows the schematic representation of local lattice distortion around bound hole polaron during the optical transition. (b) Schematic representation of corresponding Frank-Condon mechanism for optical transition in 1D configuration coordinate diagram for acceptor impurity (X = Be, Mg, Ca, Sr, Ba, Zn, and Cd) substitution at Ga site. The vertical emission (E_{em}), absorption lines (E_{abs}), and zero-phonon line energy (E_{ZPL}) are shown along with effective phonon frequencies ($\Omega_{e/g}$).

level again, leading to luminescence lines (E_{em}). The photoexcitation and de-excitation process of electrons between the $(0/-1)$ defect level and the CBM lead to absorption and emission spectra. We calculated these vertical transition levels (E_{abs} and E_{em}) using equation S16 in SM [23]. In order to calculate the vertical transition energies, we have to consider the formation energy of charged defects in frozen configurations. Therefore, we included the spurious interaction by high-frequency dielectric constant (ϵ_∞) for neutral (containing polarization charges) and charged defects, as developed by Falletta et al. [54]. Along with transition energy, all the derived vibronic parameters related to photoexcitation are shown in Table S3 in the SM [23].

Next, we calculated the photoluminescence line shape from all the acceptor defects as shown in Fig. 4. The electron capture by all defects corresponds to luminescence lines peaking
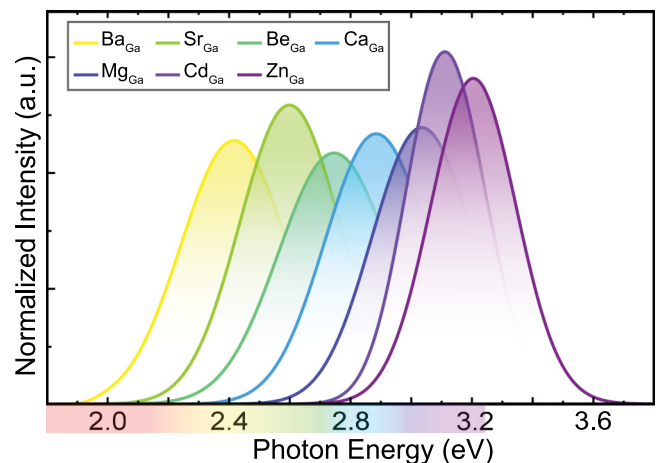
FIG. 4. Broad luminescence line shape for all acceptor impurities. The peak positions of photoluminescence for electron capture by bound hole polarons remain in the visible range of optical spectra.

at the visible region in the range of 2.41–4.17 eV. The peak position of the photoluminescence line from Gr. II Zn and Cd defects are in the blue region of the spectra at 3.21 and 3.11 eV, respectively. On the other hand, Ba_{Ga} exhibits a yellow photoluminescence line at 2.41 eV. This is because of the deepest nature of the $(0/-1)$ acceptor level, corresponding to a low ZPL at 3.07 eV. The effective ground and excited state phonon frequencies for all optical transitions are in the range of 20–40 meV, and large mass-weighted lattice distortion is between 1.84 and 4.07 $amu^{1/2}$Å. The photoluminescence lines for all the optical transitions are broad. We calculated the FWHM to determine the broadness of the photoluminescence lines. The luminescence lines for electron capture of free hole polaron are broad in nature (FWHM of 300 meV), as discussed earlier. The broadness further increases when hole polaron is facilitated by acceptor dopants (FWHM in the range of 310–440 meV; Table S3 in the SM [23]). The increase in broadness signifies that the optical transition is accompanied by larger lattice distortion. Therefore, the increased FWHM for photoluminescence transition involving self-trapped hole with dopants suggests that the hole trapping is more localized, accompanied by larger lattice distortion. This in turn, also confirms that the localized nature of bound hole polaron is responsible for deep nature of the acceptor dopants. Therefore, careful dopant selection, while keeping in mind the parameters affecting the broad character of the spectra, can provide tunability in photoluminescence of ultra-wide-band gap semiconductors. The phenomenon of strongly Stokes-shifted emissions holds potential in the realm of white light generation. Moreover, the employment of phonon-assisted luminescence exhibits advantageous prospects in the development of nanoscale thermometers and quantum information readout.

In conclusion, we investigated the self-trapping and defect-related photoluminescence properties of lithium gallate. Our simulation shows that the small hole polaron forms accompanied by structural distortion around O-site, and is more stable than the extended Bloch-like state. After electron capture from the CBM to the hole polaron, the self-trapped hole undergoes large Frank-Condon relaxation, which leads to a broad photoluminescence peak at 4.17 eV. All the deep acceptor defects serve as source of additional stability to the bound polarons, which causes broad luminescence line, peaking in the range of ultraviolet to visible spectrum (2.4 to 3.2 eV). Our understanding of the general mechanism underlying broad photoluminescence can aid in the device integration of deep defects in ultra-wide-band gap semiconductors for superior optoelectronic applications.

[1] J. Tsao, S. Chowdhury, M. Hollis, D. Jena, N. Johnson, K. Jones, R. Kaplar, S. Rajan, C. Van de Walle, E. Bellotti *et al.*, Ultrawide-bandgap semiconductors: Research opportunities and challenges, Adv. Electron. Mater. **4**, 1600501 (2018).

[2] J. Xu, W. Zheng, and F. Huang, Gallium oxide solar-blind ultraviolet photodetectors: A review, J. Mater. Chem. C **7**, 8753 (2019).

[3] C. Zhou, Q. Ai, X. Chen, X. Gao, K. Liu, and D. Shen, Ultraviolet photodetectors based on wide bandgap oxide semiconductor films, Chin. Phys. B **28**, 048503 (2019).

[4] K. Lin, J. Xing, L. N. Quan, F. De Arquer, X. Gong, J. Lu, L. Xie, W. Zhao, D. Zhang, C. Yan *et al.*, Perovskite light-emitting diodes with external quantum efficiency exceeding 20 per cent, Nature (London) **562**, 245 (2018).

[5] Z. Chu, Q. Ye, Y. Zhao, F. Ma, Z. Yin, X. Zhang, and J. You, Perovskite light-emitting diodes with external quantum efficiency exceeding 22% via small-molecule passivation, Adv. Mater. **33**, 2007169 (2021).

[6] J. Luo, X. Wang, S. Li, J. Liu, Y. Guo, G. Niu, L. Yao, Y. Fu, L. Gao, Q. Dong *et al.*, Efficient and stable emission of warm-white light from lead-free halide double perovskites, Nature (London) **563**, 541 (2018).

[7] S. Kahmann, E. K. Tekelenburg, H. Duim, M. E. Kamminga, and M. A. Loi, Extrinsic nature of the broad photoluminescence in lead iodide-based Ruddlesden-Popper perovskites, Nat. Commun. **11**, 2344 (2020).

[8] Y. Chen, T. N. Tran, N. M. H. Duong, C. Li, M. Toth, C. Bradac, I. Aharonovich, A. Solntsev, and T. T. Tran, Optical thermometry with quantum emitters in hexagonal boron nitride, ACS Appl. Mater. Interfaces **12**, 25464 (2020).

[9] L. C. Bassett, A. Alkauskas, A. L. Exarhos, and K.-M. C. Fu, Quantum defects by design, Nanophotonics **8**, 1867 (2019).

[10] F. Libbi, P. M. M. C. de Melo, Z. Zanolli, M. J. Verstraete, and N. Marzari, Phonon-Assisted Luminescence in Defect Centers from Many-Body Perturbation Theory, Phys. Rev. Lett. **128**, 167401 (2022).

[11] Z. Zhou, X. Yi, P. Xiong, X. Xu, Z. Ma, and M. Peng, Cr^{3+}-free near-infrared persistent luminescence material $LiGaO_2$: Fe^{3+}: optical properties, afterglow mechanism and potential bioimaging, J. Mater. Chem. C **8**, 14100 (2020).

[12] W. Wang, W. Yang, H. Wang, and G. Li, Epitaxial growth of GaN films on unconventional oxide substrates, J. Mater. Chem. C **2**, 9342 (2014).

[13] L. Trinkler, A. Trukhin, B. Berzina, V. Korsaks, P. Ščajev, R. Nedzinskas, S. Tumėnas, M. M. C. Chou, L. Chang, and C.-A. Li, Luminescence properties of $LiGaO_2$ crystal, Opt. Mater. (Amsterdam) **69**, 449 (2017).

[14] L. Trinkler, A. Trukhin, and M. M. Chou, Comparison of luminescence in $LiGaO_2$, Al_2O_3-Ga and Al_2O_3-Li crystals, Latv. J. Phys. Technol. Sci. **55**, 4 (2018).

[15] L. Trinkler, A. Trukhin, J. Cipa, B. Berzina, V. Korsaks, M. M. Chou, and C.-A. Li, Spectral and kinetic characteristics of pyroelectric luminescence in $LiGaO_2$, Opt. Mater. (Amsterdam) **94**, 15 (2019).

[16] Y.-J. Hsiao, T.-H. Fang, L.-W. Ji, and Z.-W. Chiu, Novel photoluminescent properties of LiGaO$_2$ nanoflakes, J. Alloys Compd. **509**, 7684 (2011).

[17] T. Yanagida, Y. Fujimoto, M. Koshimizu, N. Kawano, G. Okada, and N. Kawaguchi, Comparative studies of optical and scintillation properties between LiGaO$_2$ and LiAlO$_2$ crystals, J. Phys. Soc. Jpn. **86**, 094201 (2017).

[18] M. S. Holston, I. Ferguson, N. C. Giles, J. W. McClory, D. Winarski, J. Ji, F. Selim, and L. E. Halliburton, Green luminescence from Cu-diffused LiGaO$_2$ crystals, J. Lumin. **170**, 17 (2016).

[19] C. Chen, C.-A. Li, S.-H. Yu, and M. M. Chou, Growth and characterization of β-LiGaO$_2$ single crystal, J. Cryst. Growth **402**, 325 (2014).

[20] S. Lany and A. Zunger, Polaronic hole localization and multiple hole binding of acceptors in oxide wide-gap semiconductors, Phys. Rev. B **80**, 085202 (2009).

[21] P. Deák, Q. DuyHo, F. Seemann, B. Aradi, M. Lorke, and T. Frauenheim, Choosing the correct hybrid for defect calculations: A case study on intrinsic carrier trapping in β-Ga$_2$O$_3$, Phys. Rev. B **95**, 075208 (2017).

[22] G. Kresse and J. Furthmüller, Efficient iterative schemes for ab initio total-energy calculations using a plane-wave basis set, Phys. Rev. B **54**, 11169 (1996).

[23] See Supplemental Material at http://link.aps.org/supplemental/10.1103/PhysRevB.108.L041201 for extended computational details; self-interaction correction; geometrical and electronic structures; free and bound polaron formation energies; defect formation energy; chemical potential phase diagram; vertical transition level; optical transition energy and luminescence lines; effective parameters of luminescence line shape and 1D configuration coordinate model. The Supplemental Material also contains Refs. [24–34]

[24] M. Marezio, The crystal structure of LiGaO$_2$, Acta Crystallogr. **18**, 481 (1965).

[25] M. Fuchs and M. Scheffler, *Ab initio* pseudopotentials for electronic structure calculations of poly-atomic systems using density-functional theory, Comput. Phys. Commun. **119**, 67 (1999).

[26] G. Kresse and J. Furthmüller, Efficiency of *ab initio* total energy calculations for metals and semiconductors using a plane-wave basis set, Comput. Mater. Sci. **6**, 15 (1996).

[27] P. Deák, M. Lorke, B. Aradi, and T. Frauenheim, Optimized hybrid functionals for defect calculations in semiconductors, J. Appl. Phys. **126**, 130901 (2019).

[28] H. J. Monkhorst and J. D. Pack, Special points for Brillouin-zone integrations, Phys. Rev. B **13**, 5188 (1976).

[29] S. L. Dudarev, G. A. Botton, S. Y. Savrasov, C. J. Humphreys, and A. P. Sutton, Electron-energy-loss spectra and the structural stability of nickel oxide: An LSDA + U study, Phys. Rev. B **57**, 1505 (1998).

[30] J. P. Perdew and M. Levy, Physical Content of the Exact Kohn-Sham Orbital Energies: Band Gaps and Derivative Discontinuities, Phys. Rev. Lett. **51**, 1884 (1983).

[31] L. J. Sham and M. Schlüter, Density-Functional Theory of the Energy Gap, Phys. Rev. Lett. **51**, 1888 (1983).

[32] R. W. Godby, M. Schlüter, and L. J. Sham, Accurate Exchange-Correlation Potential for Silicon and Its Discontinuity on Addition of an Electron, Phys. Rev. Lett. **56**, 2415 (1986).

[33] J. P. Perdew, K. Burke, and M. Ernzerhof, Generalized Gradient Approximation Made Simple, Phys. Rev. Lett. **77**, 3865 (1996).

[34] J. P. Perdew, K. Burke, and M. Ernzerhof, Perdew, Burke, and Ernzerhof Reply:, Phys. Rev. Lett. **80**, 891 (1998).

[35] A. Boonchun, K. Dabsamut, and W. R. Lambrecht, First-principles study of point defects in LiGaO$_2$, J. Appl. Phys. **126**, 155703 (2019).

[36] K. Dabsamut, A. Boonchun, and W. R. Lambrecht, First-principles study of *n*-and *p*-type doping opportunities in LiGaO$_2$, J. Phys. D **53**, 274002 (2020).

[37] C. A. Lenyk, M. S. Holston, B. E. Kananen, L. E. Halliburton, and N. C. Giles, Lithium and gallium vacancies in LiGaO$_2$ crystals, J. Appl. Phys. **124**, 135702 (2018).

[38] D. Skachkov, W. R. Lambrecht, K. Dabsamut, and A. Boonchun, Computational study of electron paramagnetic resonance spectra for Li and Ga vacancies in LiGaO$_2$, J. Phys. D **53**, 17LT01 (2020).

[39] B. E. Kananen, L. E. Halliburton, E. M. Scherrer, K. Stevens, G. Foundos, K. Chang, and N. C. Giles, Electron paramagnetic resonance study of neutral Mg acceptors in β-Ga$_2$O$_3$ crystals, Appl. Phys. Lett. **111**, 072102 (2017).

[40] C. Freysoldt, B. Grabowski, T. Hickel, J. Neugebauer, G. Kresse, A. Janotti, and C. G. Van de Walle, First-principles calculations for point defects in solids, Rev. Mod. Phys. **86**, 253 (2014).

[41] C. Freysoldt, J. Neugebauer, and C. G. Van de Walle, Fully *Ab Initio* Finite-Size Corrections for Charged-Defect Supercell Calculations, Phys. Rev. Lett. **102**, 016402 (2009).

[42] Y. Kumagai and F. Oba, Electrostatics-based finite-size corrections for first-principles point defect calculations, Phys. Rev. B **89**, 195205 (2014).

[43] M. E. Turiansky, A. Alkauskas, M. Engel, G. Kresse, D. Wickramaratne, J.-X. Shen, C. E. Dreyer, and C. G. Van de Walle, Nonrad: Computing nonradiative capture coefficients from first principles, Comput. Phys. Commun. **267**, 108056 (2021).

[44] A. Alkauskas, J. L. Lyons, D. Steiauf, and C. G. Van de Walle, First-Principles Calculations of Luminescence Spectrum Line Shapes for Defects in Semiconductors: The Example of GaN and ZnO, Phys. Rev. Lett. **109**, 267401 (2012).

[45] Y. K. Frodason, K. M. Johansen, T. S. Bjørheim, B. G. Svensson, and A. Alkauskas, Zn vacancy as a polaronic hole trap in ZnO, Phys. Rev. B **95**, 094105 (2017).

[46] Y. K. Frodason, K. M. Johansen, T. S. Bjørheim, B. G. Svensson, and A. Alkauskas, Zn vacancy-donor impurity complexes in ZnO, Phys. Rev. B **97**, 104109 (2018).

[47] Y. K. Frodason, K. Johansen, L. Vines, and J. Varley, Self-trapped hole and impurity-related broad luminescence in β-Ga$_2$O$_3$, J. Appl. Phys. **127**, 075701 (2020).

[48] Y. K. Frodason, K. M. Johansen, A. Alkauskas, and L. Vines, Negative-*U* and polaronic behavior of the Zn-O divacancy in ZnO, Phys. Rev. B **99**, 174106 (2019).

[49] Y. K. Frodason, K. M. Johansen, A. Galeckas, and L. Vines, Broad luminescence from donor-complexed Li$_{zn}$ and Na$_{zn}$ acceptors in ZnO, Phys. Rev. B **100**, 184102 (2019).

[50] A. Alkauskas, M. D. McCluskey, and C. G. Van de Walle, Tutorial: Defects in semiconductors-combining experiment and theory, J. Appl. Phys. **119**, 181101 (2016).

[51] D. O. Demchenko, M. Vorobiov, O. Andrieiev, T. H. Myers, and M. A. Reshchikov, Shallow and Deep States of Beryllium

Acceptor in GaN: Why Photoluminescence Experiments Do Not Reveal Small Polarons for Defects in Semiconductors, Phys. Rev. Lett. **126**, 027401 (2021).

[52] M. M. Chou, C. Chen, C. Chang, and C.-A. Li, Growth and characterization of a-plane (112̄0) GaN films on (010) LiGaO$_2$ substrate by chemical vapor deposition, J. Cryst. Growth **363**, 113 (2013).

[53] T. Huang, S. Zhou, H. Teng, H. Lin, J. Wang, P. Han, and R. Zhang, Growth and characterization of ZnO films on (001), (100) and (010) LiGaO$_2$ substrates, J. Cryst. Growth **310**, 3144 (2008).

[54] S. Falletta, J. Wiktor, and A. Pasquarello, Finite-size corrections of defect energy levels involving ionic polarization, Phys. Rev. B **102**, 041115(R) (2020).